Cell

Riboneogenesis in Yeast

Michelle F. Clasquin,[1,2] Eugene Melamud,[1,2] Alexander Singer,[3] Jessica R. Gooding,[4] Xiaohui Xu,[3] Aiping Dong,[3] Hong Cui,[3] Shawn R. Campagna,[4] Alexei Savchenko,[3] Alexander F. Yakunin,[3] Joshua D. Rabinowitz,[1,2,*] and Amy A. Caudy[1,5,*]

[1]Lewis-Sigler Institute for Integrative Genomics
[2]Department of Chemistry
Princeton University, Princeton NJ 08544, USA
[3]Department of Chemical Engineering and Applied Chemistry, Banting and Best Department of Medical Research, University of Toronto, Toronto M5G 1L6, Canada
[4]Department of Chemistry, University of Tennessee, Knoxville, TN 37996, USA
[5]Present address: Donnelly Centre for Cellular and Biomolecular Research, University of Toronto, Toronto M5S 3E1, Canada
*Correspondence: joshr@genomics.princeton.edu (J.D.R.), amy.caudy@utoronto.ca (A.A.C.)
DOI 10.1016/j.cell.2011.05.022

SUMMARY

Glucose is catabolized in yeast via two fundamental routes, glycolysis and the oxidative pentose phosphate pathway, which produces NADPH and the essential nucleotide component ribose-5-phosphate. Here, we describe riboneogenesis, a thermodynamically driven pathway that converts glycolytic intermediates into ribose-5-phosphate without production of NADPH. Riboneogenesis begins with synthesis, by the combined action of transketolase and aldolase, of the seven-carbon bisphosphorylated sugar sedoheptulose-1,7-bisphosphate. In the pathway's committed step, sedoheptulose bisphosphate is hydrolyzed to sedoheptulose-7-phosphate by the enzyme sedoheptulose-1,7-bisphosphatase (SHB17), whose activity we identified based on metabolomic analysis of the corresponding knockout strain. The crystal structure of Shb17 in complex with sedoheptulose-1,7-bisphosphate reveals that the substrate binds in the closed furan form in the active site. Sedoheptulose-7-phosphate is ultimately converted by known enzymes of the nonoxidative pentose phosphate pathway to ribose-5-phosphate. Flux through SHB17 increases when ribose demand is high relative to demand for NADPH, including during ribosome biogenesis in metabolically synchronized yeast cells.

INTRODUCTION

Eukaryotic cells consume glucose through two primary routes, glycolysis and the oxidative pentose phosphate pathway. Glycolysis produces ATP, NADH, and trioses for amino acids and glycerolipid biosynthesis. The oxidative pentose phosphate pathway generates NADPH, ribose for DNA and RNA synthesis, and erythrose for amino acid biosynthesis. The rate and direction of the glycolytic pathway are controlled by heavily regulated enzymes that catalyze strongly thermodynamically favored reactions, e.g., phosphofructokinase, fructose bisphosphatase, and pyruvate kinase. Glucose enters the oxidative pentose phosphate pathway through the committed step glucose-6-phosphate dehydrogenase. Alternatively, glycolytic intermediates can be converted into ribose by the enzymes in the nonoxidative arm of the pathway. Unlike glycolysis and the oxidative pentose phosphate pathway, the nonoxidative pentose phosphate pathway is thought to be fully reversible, as it lacks any committed (i.e., strongly thermodynamically driven) step.

The enzymatic steps in the nonoxidative pentose phosphate pathway are controversial. Though textbooks contain a reasonable sequence of mass-balanced steps catalyzed by known enzymes, their ability to account for all isotopic distributions observed has been debated (Berthon et al., 1993; McIntyre et al., 1989; Williams et al., 1987). Moreover, regulation of the pathway flux, including whether net flow is toward or away from ribose, remains poorly understood. Inputs from other pathways or alternative reaction sequences may be required to fully explain these discrepancies. These issues are clearly important, as the growth of many tumor cells requires upregulated activity of the nonoxidative pentose phosphate pathway (Deberardinis et al., 2008).

Advances in mass spectrometry permit measurement of metabolites more sensitively, specifically, and conveniently than previously possible, allowing the revisitation of fundamental questions regarding metabolic pathway architectures and regulation (Fendt et al., 2010; Nakahigashi et al., 2009; Walther et al., 2010). Untargeted methods, based on full scan mass spectrometry, can detect both known and unexpected metabolites (Allen et al., 2003; Saito et al., 2006). These untargeted methods have been applied successfully in discovery metabolite profiling, an approach that identifies the endogenous roles of enzymes by searching for metabolites that accumulate upon enzyme inhibition (Saghatelian and Cravatt, 2005). This approach has revealed that the endogenous substrates of enzymes are often not accurately predicted by in vitro activity measurements (Saghatelian et al., 2004).

In the best-characterized eukaryote *S. cerevisiae*, more than 900 genes remain uncharacterized according to the *Saccharomyces* Genome Database (SGD Project, 2010). Some of these genes likely encode enzymes catalyzing metabolic

reactions, which potentially could be revealed by discovery metabolite profiling. The availability of sequence, transcription, and proteomic data facilitates prioritization of ubiquitously expressed, widely conserved candidate enzymes of unknown function for metabolic analysis. In this study, we describe our characterization of one such enzyme, *SHB17*, an abundant budding yeast protein that links the pentose phosphate pathway and glycolysis. Shb17 is a phosphatase that catalyzes the specific dephosphorylation of the seven- and eight-carbon sugars sedoheptulose-1,7-bisphosphate (SBP) and octulose-1-8-bisphosphate (OBP). Shb17 catalyzes the committed reaction of riboneogenesis, a sequence of reactions that leads ultimately to ribose-5-phosphate production:

$$\text{fructose-6-phosphate} + \text{glyceraldehyde-3-phosphate} \leftrightarrow \text{erythrose-4-phosphate} + \text{xylulose-5-phosphate} \quad (1)$$

$$\text{erythrose-4-phosphate} + \text{dihydroxyacetone phosphate} \leftrightarrow \text{sedoheptulose-1,7-bisphosphate} \quad (2)$$

$$\text{sedoheptulose-1,7-bisphosphate} \rightarrow \text{sedoheptulose-7-phosphate} + \text{Pi} \quad (3)$$

$$\text{sedoheptulose-7-phosphate} + \text{glyceraldehyde-3-phosphate} \leftrightarrow \text{xylulose-5-phosphate} + \text{ribose-5-phosphate} \quad (4)$$

$$\text{xylulose-5-phosphate} \leftrightarrow \leftrightarrow \text{ribose-5-phosphate} \quad (5)$$

Shb17 flux (rxn 3) is altered by nutrient and growth demands. In accordance with its role in feeding carbon to the pentose phosphate pathway, expression of *SHB17* is coordinated with other enzymes in the nonoxidative PPP, including transketolase (*TKL1* and *TKL2*, rxns 1 and 4) and ribose phosphate isomerase (*RKI1*, rxn 5). These riboneogenic enzymes work in concert during times of peak nucleotide demand to convert glycolytic triose and hexose units to ribose. Riboneogenesis provides a thermodynamically driven route of ribose production uncoupled from formation of NADPH, allowing the cell to adjust the flux of carbon to ribose in response to changing conditions.

RESULTS

A Yeast shb17 Deletion Mutant Accumulates SBP and OBP

We initiated a metabolomic screen of yeast deletion mutants of genes of unknown function. Candidate genes encoding protein domains similar to enzymes were identified by comparative sequence analysis. Metabolomic phenotypes of mutant strains were measured by reverse-phase ion pairing chromatography coupled with high-resolution full-scan mass spectrometry (Lu et al., 2010). We found that deletion of *SHB17*, formerly known as the uncharacterized gene *YKR043c*, consistently led to the accumulation of four metabolites and the depletion of a fifth (Figure 1).

Candidate formulae were obtained based on exact masses and included seven- or eight-carbon mono- or bisphosphorylated sugars. The formulae were verified by labeling cells with ^{15}N and ^{13}C (Hegeman et al., 2007) and observing no shift for the nitrogen labeling and a shift of +7 or +8 daltons for the carbon labeling (for the putative seven- and eight-carbon sugars respectively). The presence of phosphate was verified based on mass spectral fragmentation to $[H_2PO_4]^-$. Collectively, the analytical data revealed that the compounds observed were seven- and eight-carbon mono- and bisphosphorylated metabolites. We hypothesized that the accumulated compounds were sedoheptulose-1-phosphate (S1P), sedoheptulose-1,7-bisphosphate (SBP), octulose-1-phosphate (O1P), and octulose-1,8-bisphosphate (OBP) and that the depleted compound was octulose-8-phosphate (O8P) (Figure 1). Standards were synthesized for S1P, SBP, and OBP, and retention time and fragmentation patterns matched to the accumulating endogenous compounds. Although we did not synthesize O1P and O8P, the location of the phosphate moiety was deduced by comparing fragmentation patterns and retention times to those obtained with S1P and S7P (Figure S1). Seven-carbon bisphosphorylated sugars were known in the KEGG database, but not thought to exist in yeast. Eight-carbon mono- and bisphosphorylated sugars were not in metabolite databases but had been proposed in older literature (Bartlett and Bucolo, 1968; Horecker et al., 1982; Paoletti et al., 1979).

Shb17 Is a Selective Sedoheptulose and Octulose Bisphosphatase

To determine which of the accumulated compounds was the endogenous substrate for Shb17, we performed biochemical assays incubating recombinant Shb17 protein with each of the candidate substrates (S1P, SBP, and OBP). Incubation with Shb17 led to depletion of SBP and OBP, but not S1P. S7P and O8P accumulated as the products of reactions with SBP and OBP, respectively. S7P is part of the nonoxidative pentose phosphate pathway, which converts ribose-5-phosphate to the glycolytic intermediates fructose-6-phosphate (F6P) and glyceraldehyde-3-phosphate (GAP). The sedoheptulose bisphosphatase activity of Shb17 is inhibited by vanadate (data not shown). Phosphate transfer to AMP or ADP was not observed.

In addition to its observed activity as a sedoheptulose bisphosphatase, Shb17 has previously been shown to exhibit phosphatase activity against the structurally similar metabolite fructose-1,6-bisphosphate (FBP) in vitro (Kuznetsova et al., 2010). FBP does not accumulate in the *shb17Δ* strain ($\log_2$[mutant/WT] = 0.048, p = 0.6). This suggests that SBP might be the more important in vivo substrate. We measured the kinetic parameters of purified Shb17 using both FBP and SBP as substrates (Figure 2 and Figure S2). Shb17 preferentially hydrolyzes SBP, with a lower K_M and higher v_{max} than observed using FBP as a substrate (Table 1). Intracellular concentrations of 19 mM FBP and 0.19 mM SBP were determined by an isotope ratio-based approach (Bennett et al., 2008). The velocity of the enzyme acting on each substrate, assuming that the in vitro measured parameters apply also in vivo, is given by Equation (6) for the example of SBP as the substrate (Webb and Dixon, 1964):

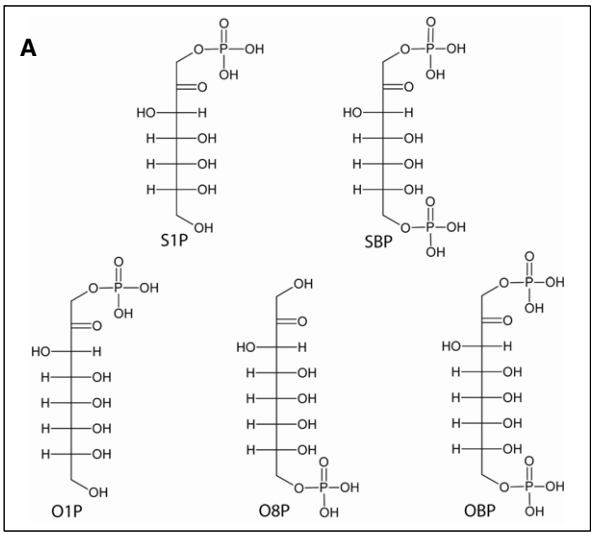

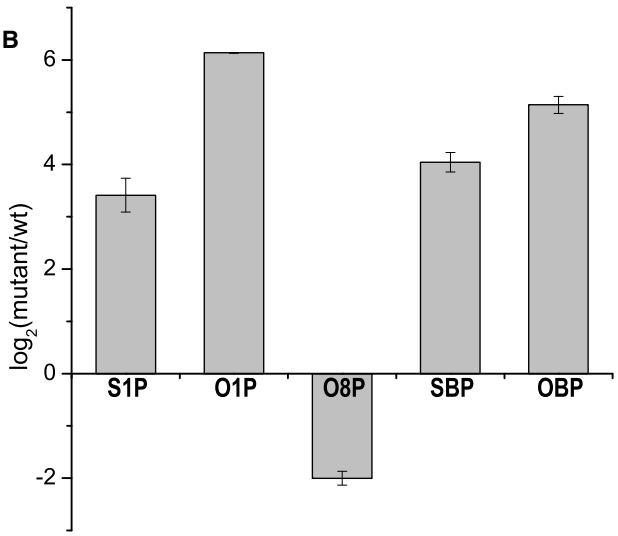

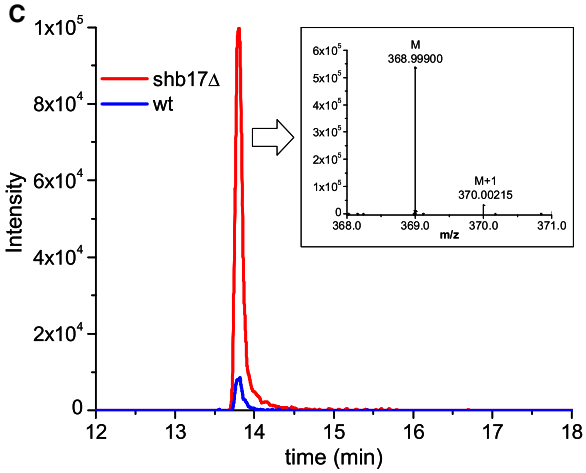

D

Compound	$[M-H]_{obs}$	ppm error	Neutral Formula
Sedoheptulose 1-phosphate (S1P)	289.03286	-0.5	$C_7H_{15}O_{10}P_1$
Octulose 1-phosphate (O1P)	319.04347	-0.3	$C_8H_{17}O_{11}P_1$
Octulose 8-phosphate (O8P)	319.04368	+0.3	$C_8H_{17}O_{11}P_1$
Sedoheptulose 1,7-bisphosphate (SBP)	368.99900	-0.9	$C_7H_{16}O_{13}P_2$
Octulose 1,8-bisphosphate (OBP)	399.00977	-0.3	$C_8H_{18}O_{14}P_2$

Figure 1. Metabolomic Phenotype of *shb17Δ*

(A) Metabolite structures associated with metabolic phenotype of *shb17Δ*. For fragmentation data confirming compound structures, see Figure S1.

(B) Relative quantitation of metabolites. Data shown are arithmetic mean ± SE of n = 4 independent biological replicates.

(C) The negative ionization mode-extracted ion chromatogram for SBP in *shb17Δ* and wild-type *S. cerevisiae*. Inset: Mass spectrum displaying the accurate mass for the parent ion (M) and natural ^{13}C abundance ion (M+1) observed for SBP in negative ionization mode via LC/Exactive Orbitrap MS.

(D) Table of [M-H] ions with altered abundance between *shb17Δ* and wild-type.

$$v_{SBP} = \frac{\frac{v_{SBP}}{K_{M\,(SBP)}}}{1 + \frac{[SBP]}{K_{M\,(SBP)}} + \frac{[FBP]}{K_{M\,(FBP)}}} \quad (6)$$

Based on Equation (6), the estimated dephosphorylation rates for SBP and FBP are similar. Using the observed concentration of 11,500 molecules of Shb17 protein per cell (Ghaemmaghami et al., 2003), we calculate that Shb17 dephosphorylates ~300,000 molecules of SBP and ~800,000 molecules of FBP per cell per minute. At an average haploid cell volume of 42 fl (Tyson et al., 1979), there are ~5 million molecules of SBP and ~500 million molecules of FBP per cell. Thus, Shb17 activity substantially affects SBP, but not FBP, levels. Moreover, typical flux through F6P is typically 10- to 20-fold greater than that through S7P in glucose-grown yeast (Kleijn et al., 2005; Wang and Hatzimanikatis, 2006). Thus, the relative contribution of Shb17 to S7P production is greater than for F6P; this was confirmed based on isotope labeling studies (see below). Thus, though the intrinsic preference of Shb17 for SBP over FBP (i.e., higher v_{max}/K_m) is substantially offset by the higher cellular concentration of FBP than SBP, the primary physiological role of Shb17 appears to be the dephosphorylation of SBP and perhaps also OBP.

Structure of Shb17-SBP Complex

Recently, Kuznetsova et al. (2010) determined the crystal structure of a catalytically inactive mutant of Shb17 (H13A) in complex

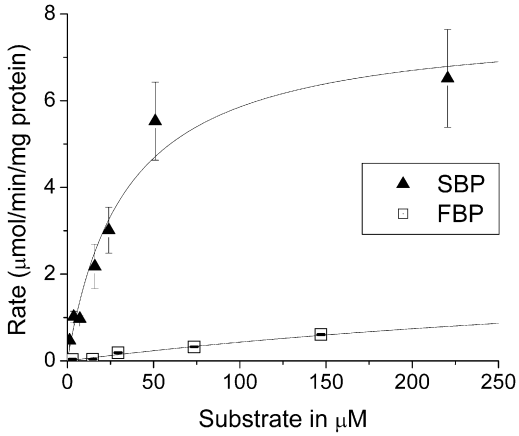

Figure 2. Hydrolysis of SBP and FBP by Purified Recombinant Shb17: Dependence on Substrate Concentration

Data are the mean ± standard error for two independent experiments. Full data for FBP are available in Figure S2.

with FBP bound in the active site. FBP was bound in an extended linear form, unlike the thermodynamically preferred cyclic β-furanose form observed in complexes with the gluconeogenic enzyme fructose bisphosphatase (Brown et al., 2009; Koerner et al., 1973). To examine the interaction of Shb17 with SBP, we cocrystallized Shb17 (H13A) with SBP and solved the structure of this complex at 2.2 Å resolution (Table S1 and Figure S3). The structure revealed a protein dimer, as in the previous crystal structures of Shb17 (Kuznetsova et al., 2010). Each monomer contains a mixed α-β structure, with a central six-stranded β sheet flanked by α helices on both sides. On one side of this central β sheet is a substrate-binding site formed by the C terminus of strand β1, the α1 helix and the β1-α1 and α1-α2 loops (residues 14–29), and the α7, α8, and α9 helices and their intervening loops (residues 101–139). Strand β7 (residues 228–234) forms another boundary for the ligand-binding site and also constitutes part of the dimer interface, hydrogen bonding with the major β sheet of the interacting monomer. The ligand sedoheptulose 1,7-bisphosphate is best modeled in its β-furanose form, which is the most common conformer of sedoheptulose and its derivatives in solution (Kuchel et al., 1990).

The Shb17 structure revealed that SBP is bound in the active site in a very similar manner to FBP (Figure 3A). This is possible because SBP is bound in a furanose (cyclic) form, and therefore it has almost the same length as FBP (the distances between the P1 and P2 phosphorus atoms are 10.7 Å and 10.6 Å, respectively). The SBP molecule is coordinated by positively charged residues on each end of the binding site that position the two terminal phosphate groups. The C1 phosphate group (P1) that is hydrolyzed by the enzyme is highly buried and held in position by hydrogen bonds and salt bridges from the side chains of R12, R69, and H176 (H13 would presumably also form a salt bridge in the wild-type enzyme) (Figure 3B). The C7 phosphate (P2) is in contact with the side chains of H178 and R181, and the side chain of H244 from the second molecule in the asymmetric unit hydrogen bonds to the C7 phosphate group. The phenyl ring of Y24 lies underneath the ligand to form a platform for the sugar molecule. In the β-furanose conformation, the C2 and C3 hydroxyl groups point into the protein and away from the solvent, each forming two hydrogen bonds with the protein. The hydroxyl group of Y102 contributes one hydrogen bond each to the C2 and C3 OH. In addition, the E99 carboxyl group and the T25 backbone amide hydrogen bond to the C2 and C3 hydroxyl group, respectively. The C4 hydroxyl group points toward the solvent and makes no direct hydrogen-bonding contacts with the protein. In addition, the Shb17-SBP structure revealed the presence of an additional density close to the side chains of the conserved T16 and T25 (2.2 Å and 3.2 Å) and to the P1 oxygen (2.9 Å), which was interpreted as an Mg^{2+} cation (Figure 3B). This type of Mg^{2+} coordination is very similar to that found in the regulatory and dynamin-like GTPases/ATPases, where Mg^{2+} is not required for substrate hydrolysis but contributes to the phosphate coordination (Daumke et al., 2007; Ruthard et al., 2001; Zhang et al., 2000). There is a similar density at this position in the structure of the Shb17 complex with FBP, which was annotated as a water molecule (Figure 3C), but potentially it might also represent a metal ion. Therefore, although Shb17 and other members of the histidine phosphatase superfamily are known to be metal-independent enzymes, it is possible that some of them can use Mg^{2+} for the cleavable phosphate coordination and charge neutralization.

Overall, the structures of Shb17 complexed with SBP or FBP revealed similar positioning of the active site residues, suggesting that both substrates are hydrolyzed using the same mechanism. Compared to the structure of the Shb17-FBP complex, however, Shb17 makes an additional interaction with SBP between the C3-OH of SBP and the Y102 of the protein and between the 1-phosphate and R12of the protein. These hydrogen bonds, in addition to the more favorable sugar conformation, presumably account for the increased affinity of Shb17 for SBP relative to FBP.

Sedoheptulose 1,7-Bisphosphate Is Synthesized In Vivo by Fructose Bisphosphate Aldolase

There are two likely routes for in vivo synthesis of sedoheptulose 1,7-bisphosphate. The first involves formation of SBP by the phosphorylation of S1P, which also accumulates in *shb17Δ*. The second is via the aldol addition of dihydroxyacetone-phosphate

Table 1. Kinetic Parameters of Shb17 with FBP and SBP as Substrates

	K_M	v_{max}	v_{max}/K_M	Intracellular Concentration	Intracellular Concentration, 95% Confidence Interval
Substrate	μM	μmoles/min mg protein	l/min mg protein	mM	mM
FBP	510 ± 50	2.6 ± 0.1	$5.1 \times 10^{-3} \pm 5 \times 10^{-4}$	19	19.9–20.5
SBP	34 ± 8	7.8 ± 0.7	$2.3 \times 10^{-1} \pm 6 \times 10^{-2}$	0.19	0.189–0.194

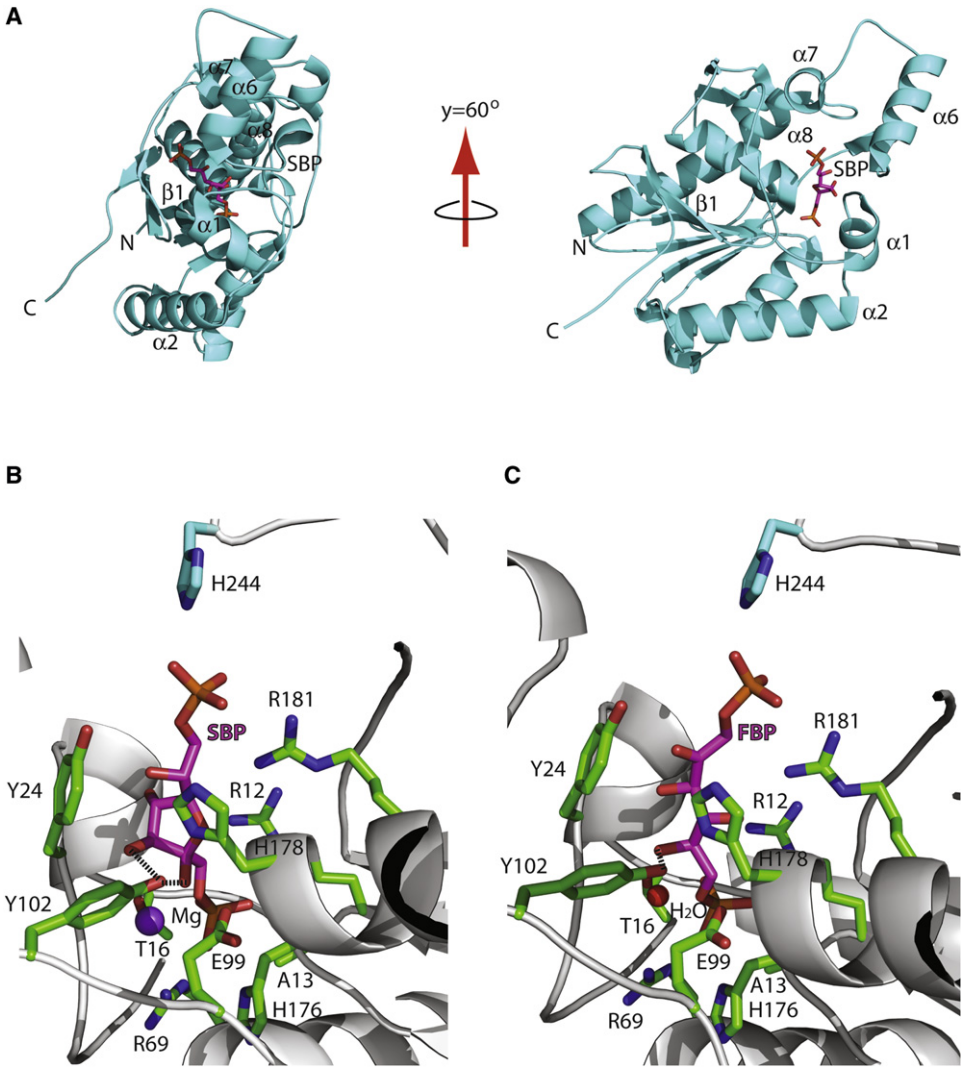

Figure 3. Structure of the Shb17/SBP Complex

(A) Overall fold of the Shb17 (H13A) in complex with SBP (PDB 3OI7, gray ribbon) shown in two orientations with secondary structural elements being labeled. The SBP molecule (magenta carbon atoms) is shown in a stick representation.

(B) Close-up view of the active site of Shb17 in complex with SBP. The side chains of residues in contact with SBP are displayed in a stick representation (green carbon atoms) and labeled. SBP is shown in a stick representation (magenta carbon atoms) and labeled, whereas the Mg^{2+} ion is shown as a purple sphere and labeled.

(C) Active site of Shb17 in complex with FBP, a similar view as (B). The red sphere denotes a water molecule. Y102 makes two hydrogen bonds with SBP, whereas only one hydrogen bond can be formed between this residue and FBP. These hydrogen bonds are shown by dashed lines in (B) and (C).

See also Figure S3 and Table S1.

(DHAP) and erythrose-4-phosphate (E4P) catalyzed by the ubiquitous glycolytic enzyme fructose bisphosphate aldolase. Similarly, octulose-1,8-bisphosphate might be synthesized by phosphorylation of O1P or by the aldol addition of DHAP and ribose-5-phosphate.

To explore these possibilities, we fed yeast a mixture of 70:30 [U-$^{13}C_6$]-glucose:unlabeled glucose. This mixture yields fully labeled and unlabeled DHAP and E4P, as well as partially labeled forms produced from scrambling reactions of the nonoxidative PPP. From these heterogeneous pools, a labeled subunit may react with an unlabeled subunit, giving rise to a partially labeled product (Szyperskia et al., 1996). In *shb17Δ* mutant cells, the predominant partially labeled forms of SBP were $^{13}C_3$ and $^{13}C_4$, consistent with SBP being synthesized by aldolase-catalyzed condensation of triose and tetrose subunits (Figure 4 and Figure S4). Similarly, $^{13}C_3$ and $^{13}C_5$ were the predominant partially labeled forms of OBP. The labeling patterns of S7P and O8P were similar to those of SBP and OBP. Partially labeled forms of S1P and O1P could not be measured due to poor signal-to-noise ratio.

To examine the role of fructose bisphosphate aldolase (FBA) in the in vivo synthesis of SBP and OBP, we decreased aldolase

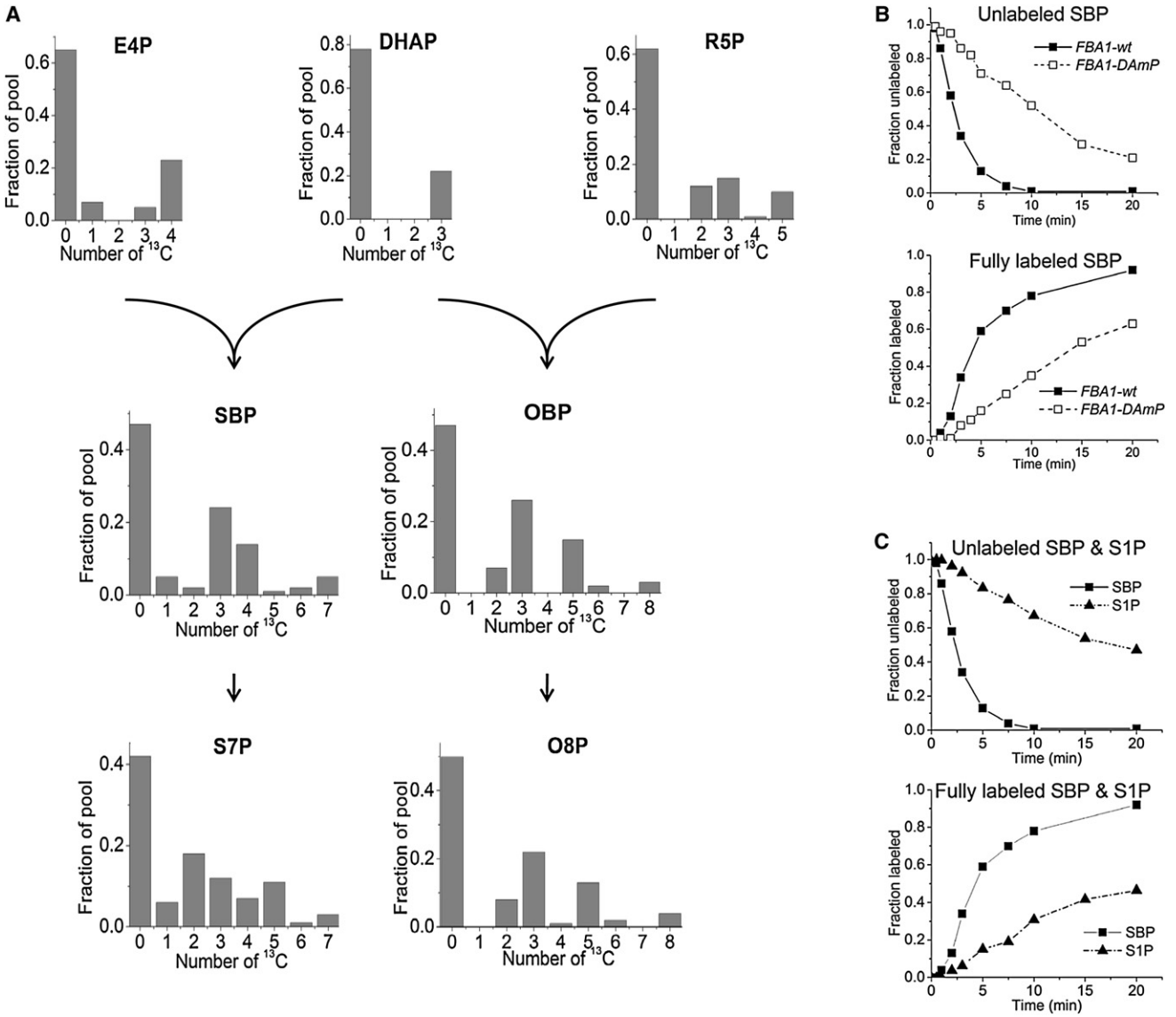

Figure 4. SBP and OBP Are Synthesized In Vivo by C_3 + C_4 and C_3 + C_5 Subunits via Fructose Bisphosphate Aldolase

(A) Cells were switched from unlabeled to 70:30 unlabeled glucose:[U-^{13}C]-glucose. Labeling patterns of erythrose-4-phosphate (E4P), dihydroxyacetone-phosphate (DHAP), ribose-5-phosphate (R5P), SBP, and OBP were measured in *shb17Δ*, where SBP and OBP accumulate and hence are more readily quantitated. The reaction products sedoheptulose-7-phosphate (S7P) and octulose 8-phosphate (O8P) were measured in wild-type (for data on S7P in *shb17Δ*, see Figure S4A). Labeling is reported 20 min after nutrient switch for all compounds except OBP, wherein data are taken at 120 min due to its slower labeling.

(B) Kinetics of labeling of SBP after switching *shb17Δ* cells with wild-type fructose bisphosphate aldolase (*FBA1-wt*) or the decreased abundance by mRNA perturbation allele (*FBA1-DAmP*) into [U-$^{13}C_6$]-glucose. For associated pool size and kinetic data, see Figures S4B and S4C.

(C) Kinetics of labeling of SBP and S1P after switching *shb17Δ* cells into [U-^{13} C_6]-glucose.

activity, encoded by the essential gene *FBA1*, by lowering its expression using a decreased abundance by mRNA perturbation (DAmP) allele (Breslow et al., 2008). The flux of glucose toward SBP and OBP was then measured by kinetic flux profiling (Yuan et al., 2008). Cells were initially grown on unlabeled media and then switched to fully isotope-labeled [U-$^{13}C_6$]-glucose. Metabolism was quenched at various time points following the switch, enabling us to monitor the rate at which isotopically labeled carbon filled each metabolite pool. We applied this method to four strains: wild-type, *shb17Δ*, *FBA1-DAmP*, and a *FBA1-DAmP/shb17Δ* double mutant. Labeling of the direct upstream intermediates of SBP, E4P, and DHAP was unaffected by the *FBA1-DAmP* allele; however, labeling of SBP and OBP was markedly slowed, verifying their cellular synthesis by aldolase (Figure 4B).

Labeling dynamics provides an additional assessment of the likelihood of SBP and OBP synthesis by aldolase versus by S1P or O1P phosphorylation, which would require that the

isotopic labeling of S1P and O1P is faster than labeling of SBP and OBP. Instead, S1P and O1P label more slowly than SBP and OBP. This slow labeling of S1P or O1P is consistent with their formation by hydrolysis of SBP and OBP, perhaps catalyzed by an unidentified phosphatase.

Quantitation of Flux through SHB17 into the Nonoxidative PPP

S7P can be produced either from SBP by Shb17 or through the canonical pentose phosphate pathway (PPP). Flux from SBP to S7P can be specifically measured based on the pseudo-steady-state labeling patterns of SBP and S7P in cells fed glucose singly labeled in its C6 position, [6-$^{13}C_1$]-glucose. Shb17, but not the canonical PPP, produces [1,7-$^{13}C_2$]-S7P from [6-$^{13}C_1$]-glucose (Figure 5A).

The metabolism of [6-$^{13}C_1$]-glucose through the PPP produces only [7-$^{13}C_1$]-S7P. PPP flux in the oxidative direction results in [6-$^{13}C_1$]-glucose-6P being decarboxylated at C1-yielding [5-$^{13}C_1$]-pentose phosphates: ribulose-5P, ribose-5P, and xylulose-5P (Xu5P). Transketolase then transfers the C1 and C2 carbons of xylulose-5P to ribose-5P, producing [7-$^{13}C_1$]-S7P and [3-$^{13}C_1$]-glyceraldehyde-3-phosphate (GAP). Nonoxidative PPP flux from glycolytic intermediates toward S7P produces the same labeling pattern. [6-$^{13}C_1$]-fructose-6P combines with [3-$^{13}C_1$]-GAP via transketolase to produce [5-$^{13}C_1$]- Xu5P and [4-$^{13}C_1$]- erythrose-4P (E4P). [4-$^{13}C_1$]- E4P then reacts with another [6-$^{13}C_1$]-fructose 6P, producing via transaldolase [7-$^{13}C_1$]-S7P.

When S7P is made via the Shb17 pathway, however, double labeling from [6-$^{13}C_1$]-glucose can occur. The origin of this double labeling is the aldolase-catalyzed condensation of [3-$^{13}C_1$]-GAP with [4-$^{13}C_1$]- E4P. This yields [1,7-$^{13}C_2$]-SBP, which is dephosphorylated by Shb17 to [1,7-$^{13}C_2$]-S7P. The steady-state fraction of [$^{13}C_2$]-S7P relative to the fraction of [$^{13}C_2$]-SBP equals the fraction of S7P produced through Shb17.

To determine flux through Shb17 by this approach, cells in yeast nitrogen base were first grown on unlabeled glucose and then switched to otherwise identical media with [6-$^{13}C_1$]-glucose for 90 min, and the ratio of the doubly labeled fractions of S7P and SBP was determined. The labeling duration was selected to allow quasi-steady-state labeling of S7P and SBP while minimizing carbon scrambling that can occur when the products of Shb17 undergo further PPP reactions (e.g., formation of doubly labeled pentoses from S7P via transketolase). To validate this strategy, we compared *shb17Δ* mutants to wild-type yeast. In wild-type, 5% of S7P was doubly labeled, whereas in *shb17Δ* cells, there was < 1% doubly labeled S7P (Figure 5B). The 5% $^{13}C_2$ labeling of S7P compared with 25% labeling of SBP implies that 20% of S7P is synthesized by dephosphorylation of SBP by Shb17 for wild-type yeast grown in minimal media. Conversely, despite the 10% doubly labeled FBP measured in wild-type yeast, no doubly labeled glucose-6-phosphate was observed, implying that hydrolysis of FBP by Shb17 is not a significant source of hexose phosphates.

Shb17 activity provides a strongly thermodynamically driven route to S7P. Accordingly, we hypothesized that its function might be to drive flux from dihydroxyacetone-phosphate and erythrose-4-phosphate toward ribose-5-phosphate. Such flux would be useful when demand for ribose is not fully met by the oxidative PPP, i.e., when demand for ribose exceeds that for NADPH. In growing yeast, NADPH is consumed substantially for amino acid, nucleic acid base, lipid, and sterol biosynthesis. Accordingly, we hypothesized that providing exogenous amino acids, nucleic acid bases, fatty acids, and sterols would increase Shb17 flux. As shown in Figure 5B, such supplementation increased flux through Shb17 from 20% in minimal medium up to almost 50% in media containing the full set of additives.

A more overt way of increasing the requirement for Shb17 flux is genetic elimination of other routes of ribose production. Deletion of glucose 6-phosphate dehydrogenase *(ZWF1)*, the enzyme that is responsible for the first committed step of the oxidative PPP, caused ~50% enhancement of Shb17 flux (Figure 5C). Deletion of the transaldolase genes *TAL1* and *NQM1*, which catalyze a portion of the nonoxidative pentose phosphate pathway, quadrupled flux through Shb17 to S7P. The combination of *zwf1Δ* mutation with *tal1Δ nqm1Δ* mutations increased flux over *zwf1Δ* alone. The overall flux through S7P is higher in *tal1Δ nqm1Δ* than in *zwf1Δ tal1Δ nqm1Δ*, but *zwf1* mutants grow slowly in the methionine-supplemented minimal media used in our flux experiments (data not shown). We anticipate that this growth defect alters overall fluxes in the cell, which is supported by prior evidence that *zwf1* mutation reduces flux to the nonoxidative pentose phosphate pathway (Zhao et al., 2004; Jeppsson et al., 2002). Simultaneous deletion of *ZWF1* and the transaldolase *TAL1* yielded cells that depend on *SHB17* for efficient growth: the triple deletion *zwf1Δ tal1Δ shb17Δ* grows slowly even on rich medium (Figure 5D). The three single mutants, double mutants with binary combinations of the mutations, or these single and double mutants in combination with mutation of the *TAL1* paralog *NQM1* (Table S3) had no significant effect on growth.

These results are consistent with three effective routes of ribose production from glucose: the oxidative PPP (via Zwf1), the canonical nonoxidative pentose phosphate pathway running in reverse (via Tal1), or riboneogenesis (via Shb17). Both of the latter two also require transketolase activity, which is itself sufficient to make ribose by converting F6P and GAP to Xu5P and E4P, with the disadvantage that Xu5P and E4P are made in stoichiometric amounts even though cellular demand for R5P exceeds that for E4P. This explains the viability but fitness defect of the *zwf1Δ tal1Δ shb17Δ* triple-deletion mutant. Consistent with the essential role for transketolase in converting S7P formed by Shb17 into ribose, the *zwf1Δ tkl1Δ tkl2Δ* triple mutation is lethal (Schaaff-Gerstenschläger et al., 1993). Moreover, in double mutants lacking all transketolase activity *(tkl1Δ tkl2Δ)*, there is no measurable flux through Shb17 (Figure 5C).

Shb17 Oscillates with Ribosomal Transcripts in the Yeast Metabolic Cycle

Further evidence supporting the role of Shb17 as a riboneogenic enzyme can be observed through analysis of periodic gene expression during the yeast metabolic cycle (Tu et al., 2005). In nutrient-limited yeast cultures, yeast cells can spontaneously synchronize their metabolism and cell cycle so that the culture alternates between respiration and fermentation. In gene expression data collected from these metabolically synchronized

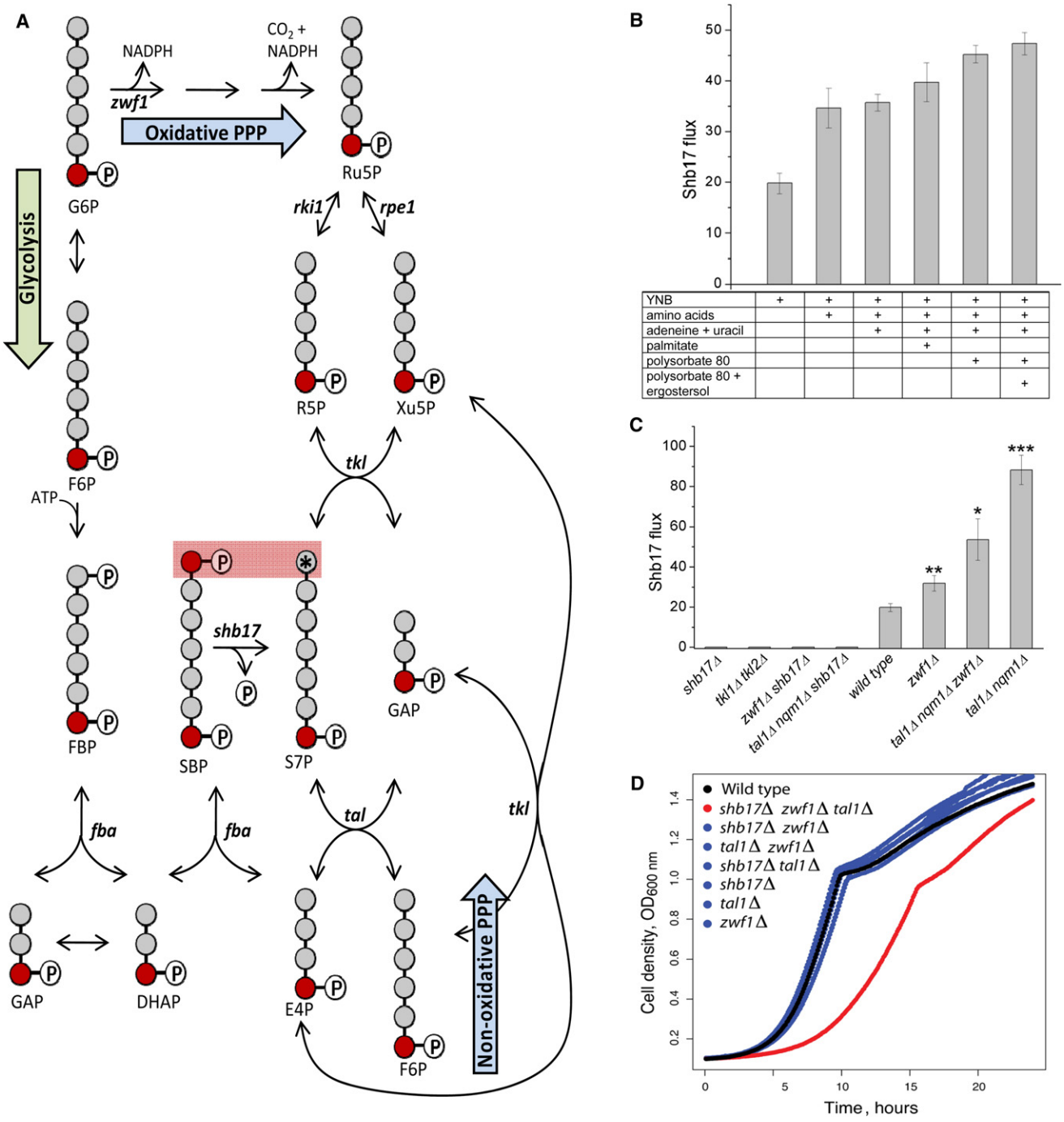

Figure 5. Shb17 Feeds Carbon into the Nonoxidative Pentose Phosphate Pathway

(A) Flux through Shb17 into S7P can be measured using [6-$^{13}C_1$]-glucose. [6-$^{13}C_1$]-glucose leads to [7-$^{13}C_1$]-S7P when S7P is made via the oxidative PPP or the nonoxidative PPP. However, when S7P is produced from SBP via Shb17, a fraction of the S7P pool is doubly labeled: [1,7-$^{13}C_2$]-S7P. Flux is calculated based on the measured isotopic distribution of SBP and S7P.

(B) Flux through Shb17 is increased by supplementation with nutrients whose endogenous production requires NADPH and thus drives oxidative PPP flux. All measurements are performed in wild-type yeast. YNB is yeast nitrogen base without amino acids plus 2% glucose. Supplementation with amino acids includes 17 amino acids. Data shown are the arithmetic mean ± SE of n = 3 technical replicates.

(C) Effects of PPP gene deletions on Shb17 flux. The flux in the mutant strains differs significantly from wild-type as calculated by a t test (*$p < 0.05$, **$p < 0.02$, ***$p < 0.001$). Deletions are: glucose 6-phosphate dehydrogenase, *zwf1Δ*; transketolase, *tkl1Δ/ tkl2Δ*; and transaldolase, *tal1Δ/nqm1Δ*. Less than 1% doubly labeled S7P was observed in any *shb17Δ* strain in all measured conditions. All strains were grown in YNB + 2% glucose and supplements as required: methionine for *zwf1Δ* and synthetic complete media, including aromatic amino acids, for *tkl1Δ/tkl2Δ*.

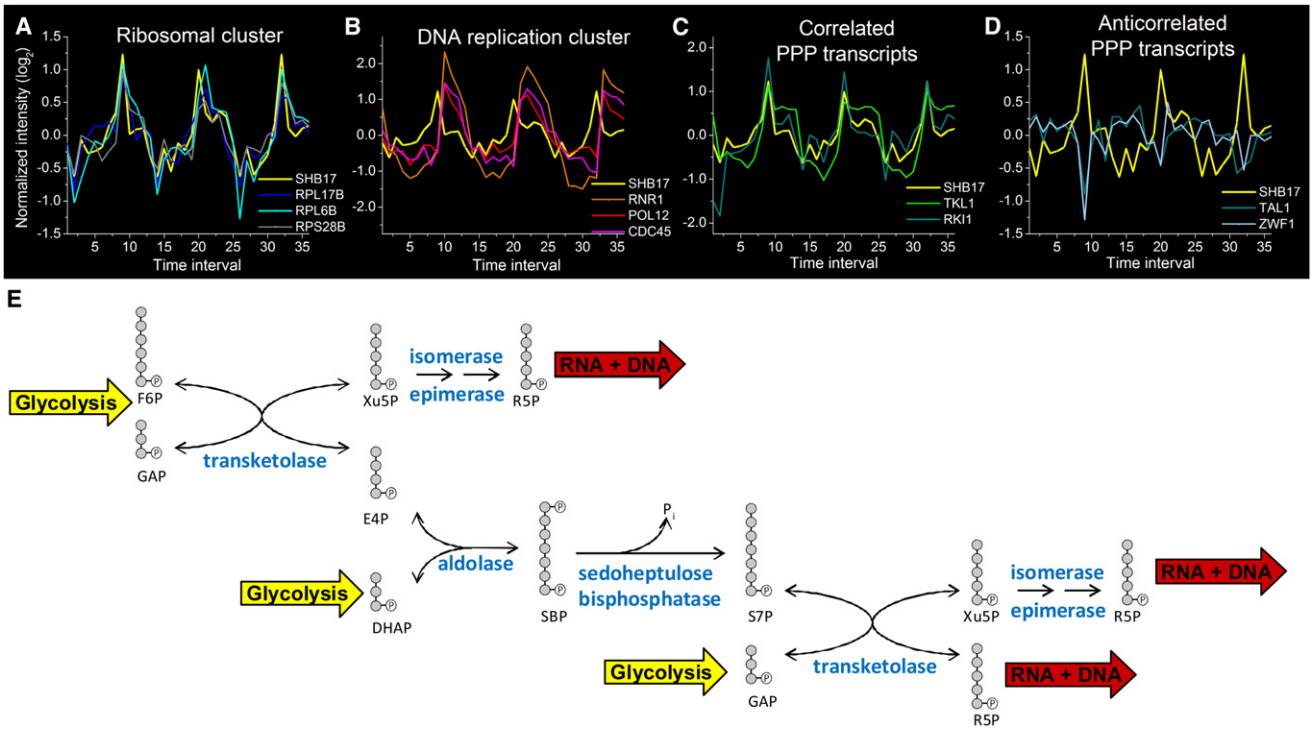

Figure 6. *SHB17* Expression Cycles in Concert with the Yeast Metabolic Cycle

(A–D) A time series of gene expression during the ~300 min yeast metabolic cycle is plotted from data presented in Tu et al. (2005), wherein each time interval represents ~25 min.

(A) *SHB17* is coexpressed with ribosomal transcripts (shown here: two components of the 60S ribosomal subunit, *RPL17B* and *RPL6B*, and one of the 40S subunit, *RPS28B*).

(B) Ribosomal protein transcript expression precedes transcripts associated with DNA replication (shown here: ribonucleotide reductase, *RNR1*, the B subunit of DNA polymerase, *POL12*, and a DNA replication initiation factor, *CDC45*).

(C) *SHB17* expression correlates with selected PPP transcripts, including transketolase (*TKL1*) and ribose 5-phosphate ketol-isomerase (*RKI1*).

(D) *SHB17* expression is anticorrelated with other PPP transcripts, including transaldolase (*TAL1*) and glucose 6-phosphate dehydrogenase (*ZWF1*). y axis displays $\log_2$ transformed intensity, with each gene median centered at 0.

(E) Riboneogenic pathway in yeast. The expression data in (A–D) suggest a coordinated role of the transketolase *TKL1*, the ribose ketoisomerase *RKI1*, and the sedoheptulose bisphosphatase *SHB17* in riboneogenesis. The aldolase *FBA1* is constitutively expressed, consistent with its central role in both glycolysis and gluconeogenesis. The ribulose epimerase *RPE1* is also continually expressed. Together, the enzymes work to shunt glycolytic intermediates to ribose. The overall scheme converts one hexose-P and three triose-P to three pentose-P units.

cells, we observed that levels of the *SHB17* transcript are correlated with expression levels of the ribosomal proteins (Figure 6A), which are expressed prior to genes required for DNA synthesis (Figure 6B) (Kudlicki et al., 2007). Thus, periodic *SHB17* expression coincides with the peak demand for ribose phosphate that occurs during ribosome biosynthesis.

Shb17 facilitates the conversion of glycolytic intermediates to pentose phosphate units. Together with aldolase and transketolase, it can convert one mole of F6P plus three moles of triose phosphate to three moles of pentose phosphate. These reactions define the previously undescribed pathway of riboneogenesis (Figure 6E). *TKL1*, the primary source of transketolase activity (Schaaff-Gerstenschläger et al., 1993), cycles concurrently with *SHB17*. The interconversion of the pentose phosphates Xu5P and R5P is achieved in two steps through the intermediate ribulose-5P (Ru5P). In the first step, Xu5P is converted to Ru5P via ribulose 5-phosphate epimerase (Rpe1). Ru5P is then converted to R5P via ribose-5-phosphate ketol-isomerase (Rki1). *RKI1* expression oscillates during the metabolic cycle in concert with *TKL1* and *SHB17*, and expression levels of *RPE1* are constant (Figure 6C).

Some of the transcripts of the PPP are anticorrelated with *SHB17* expression, including glucose 6-phosphate dehydrogenase (*ZWF1*), the first committed step of the oxidative branch of the PPP (Figure 6D). The anticorrelation of *SHB17* and *TKL1* with *ZWF1* expression suggests that riboneogenesis and the oxidative branch of the PPP are active at distinct phases of the yeast metabolic cycle.

(D) Triple deletion of the sedoheptulose bisphosphatase *SHB17*, the glucose-6-phosphate dehydrogenase *ZWF1*, and the transaldolase *TAL1* causes a growth defect. Optical density was measured during growth at 30°C in YPD. Growth data are presented in Table S3.

See also Table S2 and Table S4.

In the canonical nonoxidative PPP, transketolase and transaldolase are considered to convert two moles of F6P and one mole of triose phosphate to three moles of pentose phosphate. However, *TAL1* expression is anticorrelated with *TKL1*, *SHB17*, and *RKI1* across the yeast metabolic cycle (Figure 6D). Because *TAL1* and *TKL1* are transcribed at different points in the yeast metabolic cycle, Tal1 may not act in concert with Tkl1 for the production of ribose-5-phosphate. Instead, Shb17, Tkl1, and Rki1 presumably act in concert to produce ribose.

DISCUSSION

We report a previously unidentified enzymatic activity encoded by *SHB17* that hydrolyzes sedoheptulose-1,7-bisphosphate to sedoheptulose-7-phosphate. In combination with transketolase, ribulose-5-phosphate epimerase, and ribose-5-phosphate isomerase, the activity of *SHB17* provides a thermodynamically driven pathway from trioses produced by glycolysis to the synthesis of ribose. The flux through the Shb17 pathway is regulated in response to biosynthetic and redox demands on the cell. This alternative pathway may explain the observed increase in S7P levels when oxidative pentose phosphate activity is inhibited, where previous models had predicted a decrease in S7P (Ralser et al., 2007).

In a recent study, Kuznetsova et al. (2010) showed the ability of Shb17 to hydrolyze the homologous substrate FBP and determined the crystal structure of Shb17 in complex with it. *SHB17* deletion, however, does not alter the cellular levels of FBP, whereas it elevates those of SBP. Motivated by this metabolomic data, we demonstrate that purified Shb17 exhibits higher activity and affinity for SBP. The structure of the Shb17-SBP complex reveals that this higher affinity results from binding of SBP in the preferred β-furanose sugar conformation and from additional hydrogen bonds between Shb17 and SBP. The current study accordingly is an example of the power of combining metabolomics with structural biology to assign enzyme function and argues for similar integrated metabolomic-structural biology analysis of other enzymes of unknown function.

Sedoheptulose and octulose bisphosphates are absent from most reported pathways of microbial and animal metabolism, but metabolomic analysis in multiple species reveals that these compounds are not only present but abundant. In the distantly related fission yeast *S. pombe*, we observe the formation of doubly labeled S7P in cells fed [6-$^{13}C_1$]-glucose, suggesting a similar flux from SBP to S7P (data not shown). In *E. coli*, transaldolase mutants fed xylose employ transketolase to convert xylose to S7P, which builds up to sufficient levels to result in its phosphorylation by phosphofructokinase. The resulting SBP is then cleaved by aldolase to generate E4P and DHAP (Nakahigashi et al., 2009). Sedoheptulose and octulose compounds have also been observed in human tissues (Bartlett and Bucolo, 1960; Bucolo and Bartlett, 1960). In macrophages stimulated by endotoxin, a sedoheptulose kinase that produces S7P from sedoheptulose must be downregulated for proper activation (A. Haschemi, personal communication). Sedoheptulose-1,7-bisphosphate is elevated in tumor material (Meijer and Elias, 1984) and in oncogene-transformed cultured mouse cells (J. Fan and J.D.R., unpublished data).

Previous description of SBP and OBP in mammalian metabolism came from studies of an alternative form of the pentose phosphate pathway from the canonical reaction sequence shown in textbooks. The alternative pathway, known sometimes as the L type (in contrast to the canonical F type), is purported to be active in liver (Williams et al., 1987). Similar to the pathway described here, the L-type PPP involves interconversion of DHAP and E4P with SBP catalyzed by aldolase. The L-type PPP, however, lacks sedoheptulose-1,7-bisphosphatase activity. Instead, it relies on OBP-S7P phosphotransferase activity, which has never been purified to homogeneity or cloned genetically. Moreover, the net products and reactants of the L-type pathway are identical to those of the canonical F type. In contrast, in the pathway described here, there is net loss of one high-energy phosphate bond, which serves to provide thermodynamic driving force for ribose formation. This, in turn, conveys a physiological function, riboneogenesis.

The riboneogenic pathway has substantial similarity to the Calvin cycle, the light-independent phase of photosynthesis in which CO_2 is condensed with ribulose-1,5,-bisphosphate. In the Calvin cycle, as in riboneogenesis, sedoheptulose-1,7-bisphosphate is formed when aldolase catalyzes condensation of erythrose 4-phosphate and dihydroxyacetone phosphate. Then, a sedoheptulose bisphosphatase dephosphorylates sedoheptulose-1,7-bisphosphate to yield sedoheptulose-7-phosphate, which is converted to ribulose-1,5-bisphosphate, the substrate for addition of carbon dioxide. The plant sedoheptulose-bisphosphatases are members of the phosphoglycerate mutase family distantly related to not only Shb17, but also the fructose bisphosphatase Fbp1 and various phosphoglycerate mutases. The plant enzymes are regulated by light and are localized to the stroma of the chloroplast, where they participate in carbon fixation. In contrast, Shb17 is localized to the cytoplasm to coordinate glycolysis with the pentose phosphate pathway.

The demand for the products of the pentose phosphate pathway varies depending on cell growth rate, redox stress, and nutrient availability. It also varies during the cell cycle, as ribose is ultimately the source of ribo- and deoxyribonucleotides. Riboneogenesis allows cells to balance the demands of redox homeostasis and biosynthesis.

EXPERIMENTAL PROCEDURES

Strains and Reagents

S. cerevisiae strains were derived from the synthetic genetic analysis (SGA) deletion set (BY4743 background) (Tong et al., 2001) with the genotype *MATa ura3Δ0 leu2Δ0 his3Δ1 lys2Δ0 met15Δ0 can1Δ::LEU2*$^+$*-MFA1pr-HIS3/CAN1 ykr043cΔ::kanMX* and a *yar047cΔ::kanMX* control in the same background. Prototrophic deletions were also created by homologous recombination using the YKR043CΔ::ClonNAT allele amplified by PCR from the above deletion. Prototrophic controls were wild-type FY4 (Mat a) and FY5 (Mat α) (Winston et al., 1995). Cells were grown in minimal media comprising 6.7 g/l Difco Yeast Nitrogen Base without amino acids plus 2% (w/v) glucose. Additives were added in selected cases as described in the text and Extended Experimental Procedures. Chemistry solvents and reagents were generally the highest purity that is commercially available. Full details of source materials are available in the Extended Experimental Procedures.

Screening for Metabolic Phenotypes

Single colonies of yeast deletion and control strains (n = 4 of each) were grown overnight to saturation at 30°C in minimal medium. Cultures were set back to

OD_{600} ~0.1 in 25 ml media and allowed to grow at 30°C to midlog phase (OD_{600} between 0.4 to 0.6). Cells were harvested by vacuum filtering the cultures onto 47 mm diameter 0.45 μm nylon filters. Metabolism was quenched by quickly placing the filter cell side down in 0.8 ml of −20°C extraction solvent (40/40/20 acetonitrile/methanol/water). The cells were allowed to sit in the extraction solvent at −20°C for 15 min, at which time cells were washed off of the filter with an additional 200 μl solvent. The solvent-cell mixture was then centrifuged. The supernatant was removed and placed on ice. Pellets were resuspended in 200 μl fresh solvent, and a second extraction was performed for 15 min at 5°C. The resulting mixture was then centrifuged, and the two supernatants were combined. Aliquots were dried under N_2(g) and resuspended in HPLC-grade water prior to LC-MS analysis.

LC-MS Analysis

Full-scan LC-MS analysis, without the capability for MS/MS, was performed on an ultrahigh-performance LC system coupled by negative ion mode electrospray ionization to a standalone orbitrap mass spectrometer (Lu et al., 2010). The LC method involves reversed phase ion-pairing chromatography on a C18 column with tributylamine as the ion-pairing agent (Luo et al., 2007). The mass spectrometer was run at 1 Hz scan speed with 100,000 resolving power. Metabolites differing between wild-type and knockout strains were determined using MAVEN, an open-source LC-MS data analysis package developed in house (Melamud et al., 2010). Instrumentation and run parameters are described in detail in the Extended Experimental Procedures. LC-MS/MS data was collected in selected cases on a hybrid ion trap-orbitrap instrument.

General Synthesis of Mono and Diphosphosaccharides

A series of coupled enzymatic reactions were used to produce sedoheptulose-1,7-bisphosphate (SBP), sedoheptulose-1-phosphate (S1P), and D-*glycero*-D-*altro*-octulose-1,8-bisphosphate (OBP). In Reaction I, aldolase (4.1.2.13) cleaves fructose-1,6-bisphosphate (FBP) into glyceraldehyde-3-phosphate (GAP) and dihydroxyacetone-phosphate (DHAP). Reaction II uses aldolase (4.1.2.13) to couple glyceraldehyde-3-phosphate to erythrose-4-phosphate, erythrose, or ribose-5-phosphate to form the products SBP, S1P, or OBP, respectively. In the case of SBP, erythrose-4-phosphate is derived from the cleavage of fructose-6-phosphate by transketolase (2.2.1.1) in the presence of GAP, which produces xylulose-5-phosphate as a side product. Finally, triose phosphate isomerase (5.3.1.1) is used to facilitate conversion of DHAP to GAP, thus driving the reaction and increasing yield. These methods are modifications of previous work (Smyrniotis and Horecker, 1956; Valentin and Bolte, 1993). For detailed syntheses, see Extended Experimental Procedures.

Protein Purification and Enzymatic Assays

Initial enzymatic screens for enzymatic activity were performed using in vitro synthesized, untagged Shb17 (New England Biolabs Inc. PURExpress In Vitro Protein Synthesis Kit). Subsequent studies were performed using N-terminal His-tagged recombinant protein purified from *E. coli.* Reactions were carried out at 30°C at pH 7 and quenched using acetic acid. Reactants and products in the quenched solutions were analyzed by LC-MS. For details, see Extended Experimental Procedures.

Cell Growth Assays

Overnight cultures of the indicated mutant strains were diluted back to $OD_{600\ nm}$ ~0.1 and grown for 4 hr. These cultures were diluted to $OD_{600\ nm}$ ~0.05, and growth was monitored by measuring optical density at 600 nM in a BioTek plate reader incubated with shaking at 30°C.

Crystallography

Crystals of SHB17(H13A) were grown at room temperature by hanging-drop vapor diffusion. These crystals were soaked for 10 min in well solution plus 10 mM sedoheptulose-1,7-bisphosphate and then cryoprotected and flash frozen. The structure of SHB17(H13A) with bound sedoheptulose-1,7-bisphosphate was solved by molecular replacement from the protein coordinates of SHB17(H13A) solved with fructose-1,6-bisphosphate (PDB code 3LL4). Additional details regarding structural determination methods are described in Extended Experimental Procedures. Statistics for data collection and structure refinement are summarized in Table S1.

SUPPLEMENTAL INFORMATION

Supplemental Information includes Extended Experimental Procedures, four figures, and four tables and can be found with this article online at doi:10.1016/j.cell.2011.05.022.

ACKNOWLEDGMENTS

This research was supported by NSF Career Award MCB-0643859 to J.D.R. and NIH Grant GM071508 for the Center of Quantitative Biology at Princeton University. M.F.C. gratefully acknowledges financial support from Merck and Company through a Doctoral Research Fellowship and A.A.C. support through the Lewis-Sigler Fellows program. Additional support came from the Beckman Foundation, American Heart Association Grant 0635188N, NSF Career Award MCB-0643859, NIH Grant AI078063, the DOE Biohydrogen program (to J.D.R.), and the government of Canada through Genome Canada and the Ontario Genomics Institute (2009-OGI-ABC-1405) (to A.F.Y.). We thank Kate Kuznetsova for providing purified proteins, Wenyun Lu and Saw Kyin for assistance with mass spectrometry, and Dannie Durand and David Botstein for helpful discussions.

Received: December 15, 2010
Revised: March 2, 2011
Accepted: May 19, 2011
Published: June 9, 2011

REFERENCES

Allen, J., Davey, H.M., Broadhurst, D., Heald, J.K., Rowland, J.J., Oliver, S.G., and Kell, D.B. (2003). High-throughput classification of yeast mutants for functional genomics using metabolic footprinting. Nat. Biotechnol. *21*, 692–696.

Amberg, D.C., Burke, D.J., and Strathern, J.N. (2005). Methods in Yeast Genetics (Cold Spring Harbor, NY: Cold Spring Harbor Laboratory Press).

Bartlett, G.R., and Bucolo, G. (1960). Octulose phosphates from the human red blood cell. Biochem. Biophys. Res. Commun. *3*, 474–478.

Bartlett, G.R., and Bucolo, G. (1968). The metabolism of ribonucleoside by the human erythrocyte. Biochim. Biophys. Acta *156*, 240–253.

Bennett, B.D., Yuan, J., Kimball, E.H., and Rabinowitz, J.D. (2008). Absolute quantitation of intracellular metabolite concentrations by an isotope ratio-based approach. Nat. Protoc. *3*, 1299–1311.

Berthon, H.A., Bubb, W.A., and Kuchel, P.W. (1993). 13C n.m.r. isotopomer and computer-simulation studies of the non-oxidative pentose phosphate pathway of human erythrocytes. Biochem. J. *296*, 379–387.

Breslow, D.K., Cameron, D.M., Collins, S.R., Schuldiner, M., Stewart-Ornstein, J., Newman, H.W., Braun, S., Madhani, H.D., Krogan, N.J., and Weissman, J.S. (2008). A comprehensive strategy enabling high-resolution functional analysis of the yeast genome. Nat. Methods *5*, 711–718.

Brown, G., Singer, A., Lunin, V.V., Proudfoot, M., Skarina, T., Flick, R., Kochinyan, S., Sanishvili, R., Joachimiak, A., Edwards, A.M., et al. (2009). Structural and biochemical characterization of the type II fructose-1,6-bisphosphatase GlpX from Escherichia coli. J. Biol. Chem. *284*, 3784–3792.

Bucolo, G., and Bartlett, G.R. (1960). Sedoheptulose diphosphate formation by the human red blood cell. Biochem. Biophys. Res. Commun. *3*, 620–624.

Daumke, O., Lundmark, R., Vallis, Y., Martens, S., Butler, P.J., and McMahon, H.T. (2007). Architectural and mechanistic insights into an EHD ATPase involved in membrane remodelling. Nature *449*, 923–927.

Deberardinis, R.J., Sayed, N., Ditsworth, D., and Thompson, C.B. (2008). Brick by brick: metabolism and tumor cell growth. Curr. Opin. Genet. Dev. *18*, 54–61.

Emsley, P., and Cowtan, K. (2004). Coot: model-building tools for molecular graphics. Acta Crystallogr. D Biol. Crystallogr. *60*, 2126–2132.

Fendt, S.M., Buescher, J.M., Rudroff, F., Picotti, P., Zamboni, N., and Sauer, U. (2010). Tradeoff between enzyme and metabolite efficiency maintains metabolic homeostasis upon perturbations in enzyme capacity. Mol. Syst. Biol. *6*, 356.

Ghaemmaghami, S., Huh, W.K., Bower, K., Howson, R.W., Belle, A., Dephoure, N., O'Shea, E.K., and Weissman, J.S. (2003). Global analysis of protein expression in yeast. Nature *425*, 737–741.

Hegeman, A.D., Schulte, C.F., Cui, Q., Lewis, I.A., Huttlin, E.L., Eghbalnia, H., Harms, A.C., Ulrich, E.L., Markley, J.L., and Sussman, M.R. (2007). Stable isotope assisted assignment of elemental compositions for metabolomics. Anal. Chem. *79*, 6912–6921.

Horecker, B.L., Paoletti, F., and Williams, J.F. (1982). Occurrence and significance of octulose phosphates in liver. Ann. N. Y. Acad. Sci. *378*, 215–224.

Jeppsson, M., Johansson, B., Hahn-Hagerdal, B., and Gorwa-Grauslund, M.F. (2002). Reduced oxidative pentose phosphate pathway flux in recombinant xylose-utilizing Saccharomyces cerevisiae strains improves the ethanol yield from xylose. Appl. Environ. Microbiol. *68*, 1604–1609.

Kleijn, R.J., van Winden, W.A., van Gulik, W.M., and Heijnen, J.J. (2005). Revisiting the 13C-label distribution of the non-oxidative branch of the pentose phosphate pathway based upon kinetic and genetic evidence. FEBS J. *272*, 4970–4982.

Koerner, T.A., Jr., Cary, L.W., Bhacca, N.S., and Younathan, E.S. (1973). Tautomeric composition of D-fructose phosphates in solution by Fourier transform carbon-13 nuclear magnetic resonance. Biochem. Biophys. Res. Commun. *51*, 543–550.

Kuchel, P.W., Berthon, H.A., Bubb, W.A., McIntyre, L.M., Nygh, N.K., and Thorburn, D.R. (1990). 13C and 31P NMR studies of the pentose phosphate pathway in human erythrocytes. Biomed. Biochim. Acta. *49*, S105–S110.

Kudlicki, A., Rowicka, M., and Otwinowski, Z. (2007). SCEPTRANS: an online tool for analyzing periodic transcription in yeast. Bioinformatics *23*, 1559–1561.

Kuznetsova, E., Xu, L., Singer, A., Brown, G., Dong, A., Flick, R., Cui, H., Cuff, M., Joachimiak, A., Savchenko, A., and Yakunin, A.F. (2010). Structure and activity of the metal-independent fructose-1,6-bisphosphatase YK23 from Saccharomyces cerevisiae. J. Biol. Chem. *285*, 21049–21059.

Lu, W., Bennett, B.D., and Rabinowitz, J.D. (2008). Analytical strategies for LC-MS-based targeted metabolomics. J. Chromatogr. B Analyt. Technol. Biomed. Life Sci. *871*, 236–242.

Lu, W., Clasquin, M.F., Melamud, E., Amador-Noguez, D., Caudy, A.A., and Rabinowitz, J.D. (2010). Metabolomic analysis via reversed-phase ion-pairing liquid chromatography coupled to a stand alone orbitrap mass spectrometer. Anal. Chem. *82*, 3212–3221.

Luo, B., Groenke, K., Takors, R., Wandrey, C., and Oldiges, M. (2007). Simultaneous determination of multiple intracellular metabolites in glycolysis, pentose phosphate pathway and tricarboxylic acid cycle by liquid chromatography-mass spectrometry. J. Chromatogr. A *1147*, 153–164.

McIntyre, L.M., Thorburn, D.R., Bubb, W.A., and Kuchel, P.W. (1989). Comparison of computer simulations of the F-type and L-type non-oxidative hexose monophosphate shunts with 31P-NMR experimental data from human erythrocytes. Eur. J. Biochem. *180*, 399–420.

Meijer, A.E., and Elias, E.A. (1984). [Significance of pentosephosphate cycle capacity increase in malignant tumors for energy metabolism]. Acta Histochem. Suppl. *29*, 141–148.

Melamud, E., Vastag, L., and Rabinowitz, J.D. (2010). Metabolomic analysis and visualization engine for LC-MS data. Anal. Chem. *82*, 9818–9826.

Nakahigashi, K., Toya, Y., Ishii, N., Soga, T., Hasegawa, M., Watanabe, H., Takai, Y., Honma, M., Mori, H., and Tomita, M. (2009). Systematic phenome analysis of Escherichia coli multiple-knockout mutants reveals hidden reactions in central carbon metabolism. Mol. Syst. Biol. *5*, 306.

Paoletti, F., Williams, J.F., and Horecker, B.L. (1979). Detection and estimation of sedoheptulose and octulose mono- and bisphosphates in extracts of rat liver. Arch. Biochem. Biophys. *198*, 620–626.

Ralser, M., Wamelink, M.M., Kowald, A., Gerisch, B., Heeren, G., Struys, E.A., Klipp, E., Jakobs, C., Breitenbach, M., Lehrach, H., and Krobitsch, S. (2007). Dynamic rerouting of the carbohydrate flux is key to counteracting oxidative stress. J. Biol. *6*, 10.

Rutthard, H., Banerjee, A., and Makinen, M.W. (2001). Mg2+ is not catalytically required in the intrinsic and kirromycin-stimulated GTPase action of Thermus thermophilus EF-Tu. J. Biol. Chem. *276*, 18728–18733.

Saghatelian, A., and Cravatt, B.F. (2005). Discovery metabolite profiling—forging functional connections between the proteome and metabolome. Life Sci. *77*, 1759–1766.

Saghatelian, A., Trauger, S.A., Want, E.J., Hawkins, E.G., Siuzdak, G., and Cravatt, B.F. (2004). Assignment of endogenous substrates to enzymes by global metabolite profiling. Biochemistry *43*, 14332–14339.

Saito, N., Robert, M., Kitamura, S., Baran, R., Soga, T., Mori, H., Nishioka, T., and Tomita, M. (2006). Metabolomics approach for enzyme discovery. J. Proteome Res. *5*, 1979–1987.

Schaaff-Gerstenschläger, I., Mannhaupt, G., Vetter, I., Zimmermann, F.K., and Feldmann, H. (1993). TKL2, a second transketolase gene of Saccharomyces cerevisiae. Cloning, sequence and deletion analysis of the gene. Eur. J. Biochem. *217*, 487–492.

SGD Project. "Saccharomyces Genome Database" http://www.yeastgenome.org/ (November 16, 2010).

Smyrniotis, P.Z., and Horecker, B.L. (1956). The preparation of sedoheptulose diphosphate. J. Biol. Chem. *218*, 745–752.

Szyperskia, T., Baileyb, J.E., and Wüthrich, K. (1996). Detecting and dissecting metabolic fluxes using biosynthetic fractional 13C labeling and two-dimensional NMR spectroscopy. Trends Biotechnol. *14*, 453–459.

Tong, A.H., Evangelista, M., Parsons, A.B., Xu, H., Bader, G.D., Pagé, N., Robinson, M., Raghibizadeh, S., Hogue, C.W., Bussey, H., et al. (2001). Systematic genetic analysis with ordered arrays of yeast deletion mutants. Science *294*, 2364–2368.

Tu, B.P., Kudlicki, A., Rowicka, M., and McKnight, S.L. (2005). Logic of the yeast metabolic cycle: temporal compartmentalization of cellular processes. Science *310*, 1152–1158.

Tyson, C.B., Lord, P.G., and Wheals, A.E. (1979). Dependency of size of Saccharomyces cerevisiae cells on growth rate. J. Bacteriol. *138*, 92–98.

Valentin, M., and Bolte, J. (1993). Fructose-1,6-diphosphate aldolase from spinach leaves, a challenger for enzymatic synthesis of ketoses. Tet. Lett. *34*, 8103–8106.

Walther, T., Novo, M., Rössger, K., Létisse, F., Loret, M.O., Portais, J.C., and François, J.M. (2010). Control of ATP homeostasis during the respiro-fermentative transition in yeast. Mol. Syst. Biol. *6*, 344.

Wang, L., and Hatzimanikatis, V. (2006). Metabolic engineering under uncertainty–II: analysis of yeast metabolism. Metab. Eng. *8*, 142–159.

Webb, M., and Dixon, E.C. (1964). Enzymes, Second Edition (New York: Academic Press).

Williams, J.F., Arora, K.K., and Longenecker, J.P. (1987). The pentose pathway: a random harvest. Impediments which oppose acceptance of the classical (F-type) pentose cycle for liver, some neoplasms and photosynthetic tissue. The case for the L-type pentose pathway. Int. J. Biochem. *19*, 749–817.

Winston, F., Dollard, C., and Ricupero-Hovasse, S.L. (1995). Construction of a set of convenient Saccharomyces cerevisiae strains that are isogenic to S288C. Yeast *11*, 53–55.

Yuan, J., Bennett, B.D., and Rabinowitz, J.D. (2008). Kinetic flux profiling for quantitation of cellular metabolic fluxes. Nat. Protoc. *3*, 1328–1340.

Zhang, B., Zhang, Y., Wang, Z., and Zheng, Y. (2000). The role of Mg2+ cofactor in the guanine nucleotide exchange and GTP hydrolysis reactions of Rho family GTP-binding proteins. J. Biol. Chem. *275*, 25299–25307.

Zhao, J., Baba, T., Mori, H., and Shimizu, K. (2004). Effect of zwf gene knockout on the metabolism of Escherichia coli grown on glucose or acetate. Metab. Eng. *6*, 164–174.